33rd Annual International Conference of the IEEE EMBS
Boston, Massachusetts USA, August 30 - September 3, 2011

Comparison of TOA and RSS Based Techniques for RF Localization inside Human Tissue

Umair I. Khan, Kaveh Pahlavan, Sergey Makarov
Electrical and Computer Engineering
Worcester Polytechnic Institute
Worcester, MA, USA
{uikhan, kaveh, makarov}@wpi.edu

Abstract - **Localization inside the human body using radio frequency (RF) transmission is gaining importance in a number of applications such as Capsule Endoscopy. The accuracy of RF localization depends on the technology adopted for this purpose. The two most common RF localization technologies use received signal strength (RSS) and time-of-arrival (TOA). This paper presents a comparison of the accuracy of TOA and RSS based localization inside human tissue. Analysis of the propagation of radio waves inside the human body is extremely challenging and computationally intensive. We use our proprietary finite difference time domain (FDTD) technique algorithm reported in [1] to simulate waveform transmissions inside the human body, which is almost 60 times faster than commercially available solvers used for similar purposes. The RSS and TOA of the waveforms are extracted for localization and the accuracies of the two methods are compared. The accuracy of each technique is compared with traditional CRLB commonly used for calculation of bounds for the performance of localization techniques.**

I. INTRODUCTION AND RELATED WORK

In the past decade miniaturization and declining costs of semiconductor devices have allowed design of small, low-cost computing and wireless communication devices. These are used as sensors in a variety of popular wireless networking applications and this trend is expected to continue in the next two decades. One of the most promising areas of economic growth associated with this industry is being termed *wireless Body Area Networks* (BAN) or *Body Sensor Networks* (BSN). These networks are expected to connect wearable and implantable sensory nodes together and with the Internet as part of the emerging "Internet of Things" These networks will support numerous applications ranging from traditional externally mounted temperature meters or implanted pacemakers to emerging blood pressure sensors, eye pressure sensors for glaucoma, and smart pills for precision drug delivery. A number of technical challenges regarding size and cost, energy requirements, and wireless communication technology are under investigation and at the core of these investigations is the importance of understanding radio propagation in and around the human body.

In January 2003, the Federal Communication Commission (FCC) defined a standard for medical implant communication, allowing two-way communication between implants in a frequency band at 402-405 MHz with a maximum signal bandwidth of 300 kHz. This band is called the *Medical Implant Communication Services* (MICS) band. The MedRadio band that was released in Sep 4, 2009 to extend MICS to 401-406MHz and the IEEE 802.15.6 Working Group was formed to address standardization of these emerging technologies. As part of its deliberations, the IEEE 802.15.6 Working Group defines the models for characteristics of the medium for wearable and implanted sensor networks.

Recently, Wireless Capsule Endoscopy (WCE) has become a very popular method for diagnosis of the human gastrointestinal (GI) tract. The technique is non-invasive and more precise, portable and personal as compared with traditional scope-based endoscopy. Capsule Localization plays a crucial role in the process of diagnosis and follow up interventions since doctors need to know the position and orientation of the capsule when images are collected. Various technologies for localization of the capsule have been explored in feasibility studies. [2]

The human body is not an ideal medium for RF wave transmission. It is partially conductive and consists of materials of different dielectric constants, thicknesses, and characteristic impedances. Therefore, depending on the frequency of operation, the human body can exhibit high power absorption, central frequency shift, and radiation pattern disruption. The absorption effects vary in magnitude with both frequency of the applied field and the characteristics of the tissue. The shadowing should be considered for stationary and non-stationary position of body. Because of multipath reflections, the channel response of a BAN channel resembles a series of pulses. In practice the number of pulses that can be distinguished is very large and depends on the time resolution of the measurement system. The power delay profile of the channel is an average power of the signal as a function of the delay with respect to the first arrival path. [3]

II. INTRODUCTION TO FDTD

The lumped port model in FDTD, used in our sensor design, is shown in Figure 1 [1]. It occupies one unit cell. The generator circuit includes the open gap antenna feed with the electric field $E_z(t, x_e, y_e, z_e)$, which is updated based on the Maxwell equations in free space. We apply KVL to loop 1 as indicated in Figure 1. This yield:

$$-V_g(t) + R_g I_g(t) - \Delta z E_z(t, x_e, y_e, z_e) = 0 \quad (1)$$

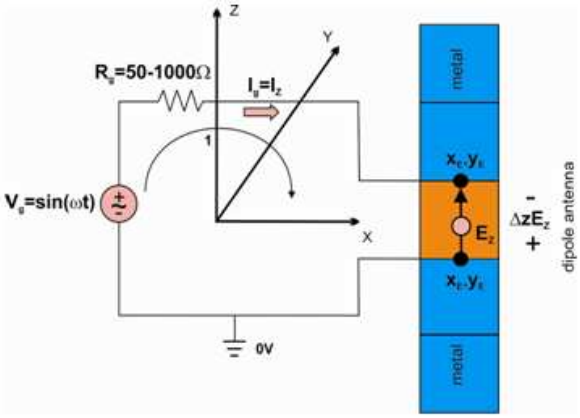

Figure 1 FDTD port model corresponding to an excitation source

Solving Equation (1) for the current results in

$$I_g(t) = \frac{1}{R_g} V_g(t) + \frac{\Delta z}{R_g} E_z(t, x_e, y_e, z_e) \quad (2)$$

The FDTD version of Equation (2) becomes

$$I^{n}_{z\,k,m,p+1/2} = \frac{\Delta z}{R_g} E^{n}_{z\,k,m,p+1/2} + \frac{1}{R_G} V^{n} \quad (3)$$

where *k, m, p* are grid-related integers and *n* is discrete time. This yields a numerically stable algorithm for arbitrary positive resistance values. Using Ampere's law with an impressed current source from Equation (3) one has the fully explicit formulation for the source

$$E_z^{n+1} = e_{S1} E_z^{n} + e_{S2} \Delta_x H_y^{n+1/2} - e_{S2} \Delta_y H_x^{n+1/2} - e_{S3} \frac{1}{2}\left(V^{n+1} + V^{n}\right) \quad (4)$$

where

$$\sigma = \frac{\Delta z}{R_g \Delta x \Delta y} = \frac{1}{R_g \Delta}, \quad e_{S1} = \frac{1 - \frac{\Delta t \sigma}{2\varepsilon_{k,m}}}{1 + \frac{\Delta t \sigma}{2\varepsilon_{k,m}}}, \quad e_{S2} = \frac{\frac{\Delta t}{\varepsilon_{k,m} \Delta}}{1 + \frac{\Delta t \sigma}{2\varepsilon_{k,m}}}, \quad e_{S3} = \frac{\frac{\Delta t \sigma}{\varepsilon_{k,m} \Delta}}{1 + \frac{\Delta t \sigma}{2\varepsilon_{k,m}}} \quad (5)$$

with $\Delta = \Delta x = \Delta y = \Delta z$ being the unit cell size. Equation (3) gives us the generator current in the time domain. For the receiver, Equations (3) – (5) again apply, but with the voltage source set equal to zero. The receiver voltage is thus given by

$$V_L(t) = R_L I_L(t) \quad (6)$$

The transmitted and received powers are found in the same fashion.

III. TOA BASED TECHNIQUES AND SIMULATION

The human body channel suffers from severe multipath propagation and heavy shadow fading conditions so that measurements for localization are far from accurate in many instances. TOA and received signal strength (RSS) estimation are therefore susceptible to large errors due to undesirable multipath conditions. To accurately estimate TOA in indoor areas, we need to resort to different frequencies of operation and more complex signaling formats and signal processing techniques that can resolve the problems. The behavior of a TOA sensor in human body multipath propagation is highly sensitive to the bandwidth of the sensor [2]. In practice, bandwidth is limited, and the received signal comprise a number of pulses whose amplitudes and arrival times are the same as impulses but they are shaped pulse. The superposition of all these pulse shapes forms the received signal, which we refer to as the channel profile. A common practice is to estimate the location of the direct path (DP) as the location of the peak of the first path that is the estimated TOA. In a single path environment, the actual expected and the estimated direct paths are the same. In multipath conditions, however, the peak of the channel profile gets shifted from the expected TOA, resulting in a TOA estimation error caused by the multipath condition. We refer to the distance error caused by erroneous estimate of the TOA as the *distance measurement error*. For a given multipath condition we expect that as we increase the bandwidth the distance measurement error becomes smaller. The UWB systems, which exploit bandwidths in excess of 1GHz, have attracted considerable attentions in indoor areas as a means of measuring accurate TOA for indoor geolocation applications cannot be used around the human body due to the FCC frequency limitations mentioned in the first section. However for the sake of research, we have used higher bandwidth pulses which may have higher frequency content. This is just to check whether TOA can be used as a good measure for distances between two sensors in and around the human body. The input pulse used is a Hanning pulse to match it with the window used in the Inverse Fourier Transform of the data taken from the network analyzer being used in the lab for real measurements.

Figure 2 shows an FDTD simulation in MATLAB. This figure shows electric field distribution around the human body model with the transmitter and receiver sensors at positions and **a** and **b** respectively, which are 5 cm apart. As shown in the figure (right bottom), the TOA of the "first

path" arrives at 0.2277 ns, which roughly translates to 6.83 cm, i.e. a distance measurement error of 1.83 cm. Notice, also, on the right side that the actual sensors for the simulation are not visible. This is because we tried to model a point source (with one FDTD cell) instead of a dipole antenna to eliminate the effects that maybe caused by impedance matching. However, it is not possible to model a perfect point (soft) source in MATLAB using FDTD, and that is why we can see the dip after the pulse is received. But if we plot the normalized power received, the negative region of that plot will be eliminated when the voltage is squared.

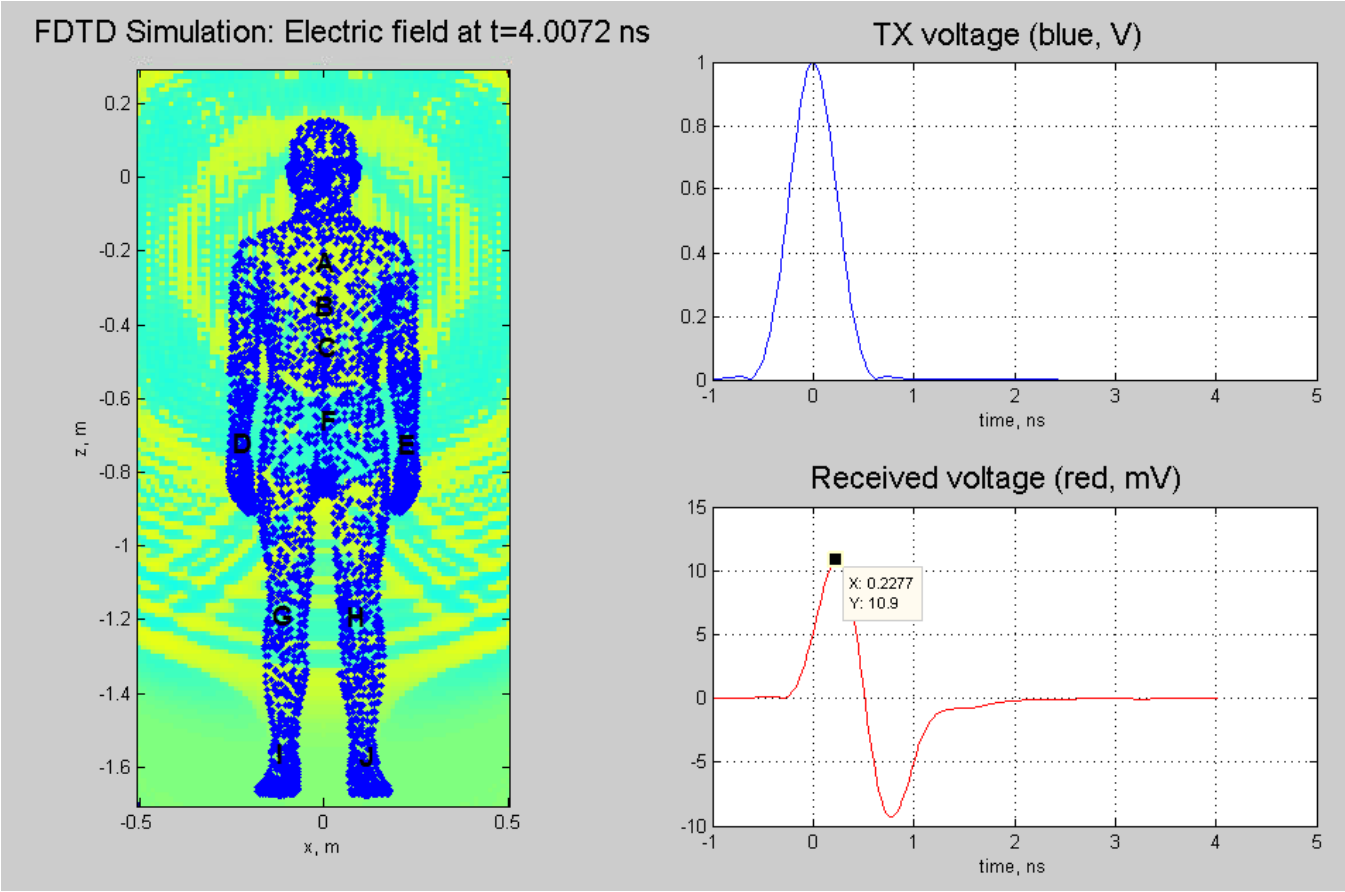

Figure 2 Left: Map of where the sensors were placed; Right: Transmitted (top) and received (bottom) voltages vs. time

IV. COMPARISON BETWEEN TOA RESULTS AND PUBLISHED PATH-LOSS MODELS USING RSS

A number of such simulations were carried out with the transmitter kept at position **a** and the position of the receiver was varied from positions **b** to **j**. One such simulation was run where the position of the transmitter was at **d** and the receiver was kept at position **e**. The received pulse from this simulation is shown in Figure 3. This verifies the multipath effect due to the waves traveling in different media. This is because while the other simulations were performed with both the sensors inside the homogenous body model and the waves did not have to travel outside that body, there weren't any detected second or third paths, but since in this simulation there was a change of mediums between the sensors, we can see more than one paths at the receiver.

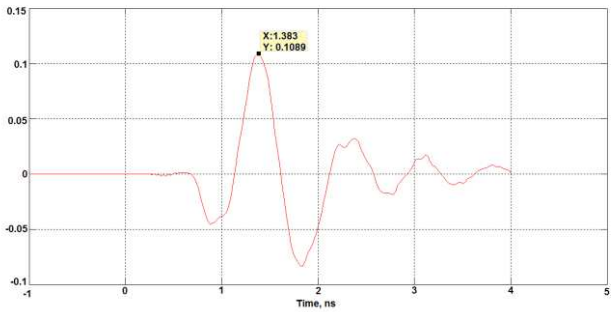

Figure 3: Received pulse (V) with transmitter and receiver sensors at positions **d** and **e** respectively.

All these simulations were then used to plot a distance vs. TOA plot to assess deviations of the plotted points from a straight line representing the ideal TOA for each distance. Figure 4 shows this plot.

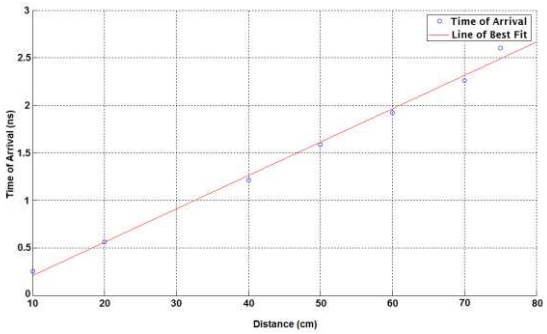

Figure 4: Time of Arrival vs. distance for various sensor positions

This plot was then compared to a plot of the same distance range obtained from the channel model described by the NIST in one of their papers that used FEM for path-loss modeling [4]. The model as shown in the paper is shown in Equation (7) and Table I, where σ_s is the variance of the normal random variable S.

$$PL(r) = PL_0 + 10\alpha log(r/r_0) + S \tag{7}$$

TABLE I
MODEL OF IMPLANT TO BODY SURFACE CM2 FOR 402-405MHZ

Implant to Body Surface	$PL(d_0)(dB)$	α	$\sigma_s(dB)$
Deep Tissue	47.14	4.26	7.85
Near Surface	49.81	4.22	6.81

The plot obtained from this model is shown in Figure 4.

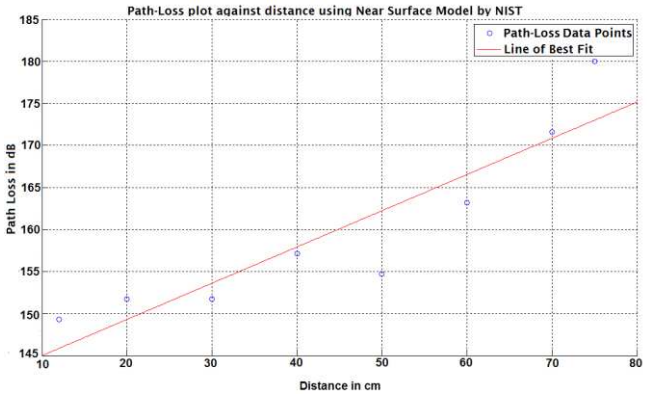

Figure 5: Plot obtained from the path-loss model in [4]

The standard deviation per dB of the Path-loss model came out to be 15.575/50 = 0.3115. While, the standard deviation per ns of the TOA model came out to be 0.361004/1.4 = 0.25786. Hence, for now, the Path-loss model seems to be more accurate. More detailed simulations are underway to improve the accuracy of the TOA model.

To estimate the distance from the TOA plot shown in Fig. 4, we used Equation (8) [5].

$$v(\omega) = \frac{c}{\sqrt{\varepsilon_r(\omega)}}, \tag{8}$$

From the slope of the TOA vs. distance line, the ε_r came out to be 1.336. This value was also used to estimate the measured value for a distance of 5 cm between the sensors, mentioned in section II. Figure 6 shows the distance measurement error plot obtained from the simulations carried out. It can be seen that the distance measurement error (given in millimeters) increases linearly with distance.

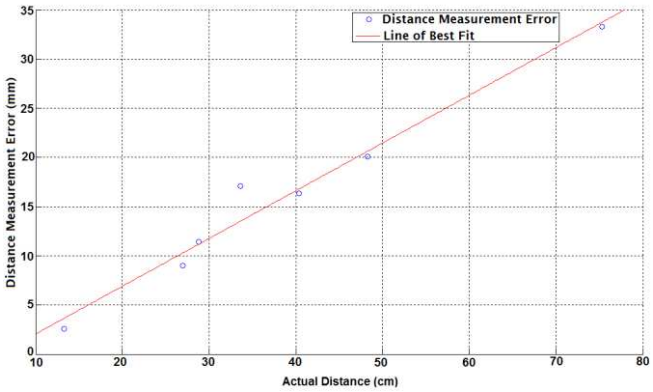

Figure 6: Distance Measurement Error from TOA for each sensor position

V. CRLB AND RANGING ACCURACY OF TOA VS. RSS

Another metric to compare the accuracy of TOA and RSS based localization methods is their respective Cramer-Rao Lower Bounds (CRLB) [6]. The CRLB of a deterministic parameter expresses a lower bound on the variance of its estimators. The CRLB on the variance of the ranging error for TOA systems is given by:

$$\sigma_D^2 \geq \frac{1}{8\pi^2}\frac{1}{SNR}\frac{1}{TW}\frac{1}{f_0^2}\frac{1}{1+\frac{W^2}{12 f_0^2}} \tag{9}$$

where T is the observation time, SNR is the Signal-To-Noise-Ratio, f_0 is the center frequency of operation and W is the bandwidth of the system. For the operating frequency, bandwidth and SNR used in GPS systems this bound shows us that accuracies around several meters is achievable if we can wait for a few minutes. If we want to extend this technology to the human body we have three challenges (1) we need more precision to identify objects inside the body (2) we need to cope with the additional path loss to into the tissue within reasonable measurement times (3) we need algorithms to cope with possible multipath conditions.

In the case of RSS, the CRLB of the ranging error, using Equation (7) to relate the distance to the power, is given by:

$$\sigma_D^2 \geq \frac{(\ln 10)^2}{100} \frac{\sigma_{sh}^2}{\alpha} d \quad (10)$$

in which σ_{sh} is the standard deviation of the shadow fading. The distance power gradient (α) would greatly vary for different parts of the human tissue as already shown in Figure 5. Also, using Equation 10, the distance measurement error for RSS comes to the order of the distance between the transmitter and receiver, which would not be acceptable for the millimeter level accuracy required inside the human body.

To check this claim, we plotted the RSS from our simulations for each of the sensor positions shown in Figure 2. This plot is shown in Figure 7, and the α obtained from this plot came out to be 4.59, which is comparable to the model in Table I.

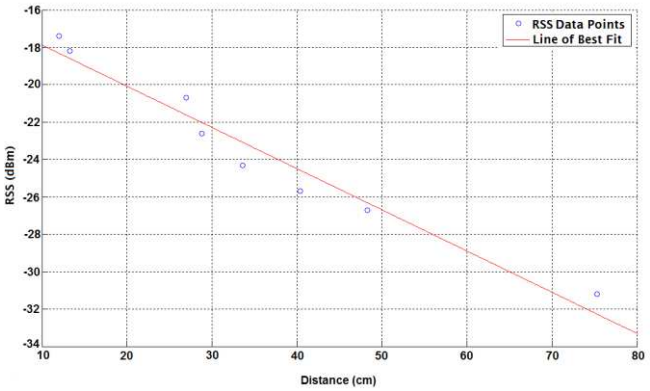

Figure 7: RSS vs. Distance plot for each sensor position

The values plotted in Figure 7 were then plugged into Equation (7) and the distance measurement error for RSS was plotted. This plot is shown in Figure 8. Notice that the errors obtained from TOA, shown in Figure 6, are in the millimeter range and the highest value is 3.5 cm, while the ones shown in Figure 8 are in cm, with the highest value being 5.1 cm. This confirms that ranging using RSS has larger errors than its TOA counterpart. To further confirm this, if we plug in the values given in TABLE I into Equation (10), at a distance of 50 cm, we can find the CRLB of RSS for the variance was in the range of 0.0699 and 0.427 dB; while the CRLB for TOA using Equation (9) came out to be 1.1388 x 10^{-12} ns.

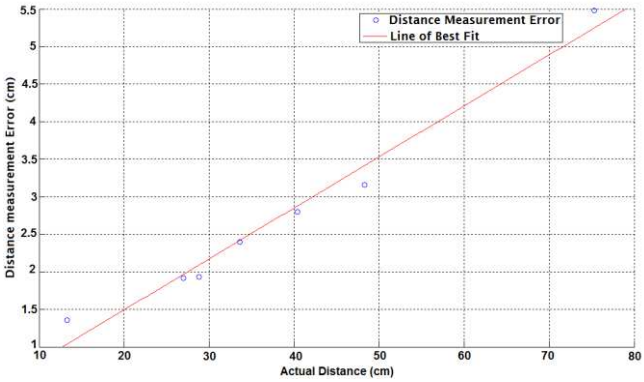

Figure 8: Distance Measurement Error from RSS for each sensor position

VI. SOURCES OF ERROR IN LOCALIZATION

The CRLB provides the ultimate measure of accuracy for ranging, but for digital systems inside the body, we get sampling and quantization errors. It may be of some interest as to why the standard deviation for TOA that was calculated experimentally in Section IV is about 10^{12} times larger than the CRLB calculated in Section V. One of the reasons for this could be that the multipath characteristics of the human body can only be truly modeled with a non-homogenous body model. Work is being done in order to import individual organs to the MATLAB FDTD solver developed by the research team. Once this is achieved and all the organs have been assigned different values of dielectric constants and conductivity, can we see the true multipath effects of the human body. Another reason for an error in TOA in real measurements could be the movement in the human body. This can change the distance between the two sensors. Figure 9 shows that, if sensor a is located on the chest and sensor b on the belt, the simple movement of raising both hands can cause a change of 3.2 cm (from 31 cm to 34.2 cm) and in the distance between them. The change in distance between these same sensors when the body is in the running position is 2.1 cm (from 31 cm to 28.9 cm). So if the position of the surface sensor changes with simple bodily movements, there will be much larger errors in measuring the distance between these sensors and an endoscopy capsule traveling inside the GI tract. Further results that may eliminate these problems will be presented at the conference.

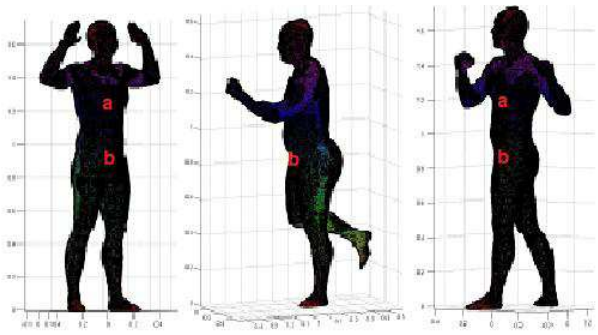

Figure 9: Change in distance of two sensors due to the movement of the body

VII. CONCLUSIONS

The study conducted in this paper verifies that Time of Arrival is a more accurate measure of distance between two sensors in a fading environment than the Received Signal Strength. We first demonstrated by comparing a plot obtained from a published RSS model with our TOA results gathered from simulations run on our proprietary FDTD algorithm, which requires less computational resources than commercially available FEM solvers used for similar simulations. We then verified this observation by using CRLB equations given in the literature and substituting the values obtained from the data of our own FDTD simulations for both RSS and TOA techniques. Finally we investigated possible reasons for the discrepancies between the simulated and calculated values of the variance for TOA and RSS techniques.

VII. ACKNOWLEDGEMENTS

We would like to acknowledge the efforts of Dr. Allen Levesque for his invaluable comments on the content of this paper. We would also like to thank Gregory Noetscher for his contributions towards this research.

[1] S. Makarov, U. Khan, M. Islam, R. Ludwig and K. Pahlavan "On Accuracy of Simple FDTD Models for the Simulation of Human Body Path Loss" *in the 2011 IEEE Sensor Applications Symposium.*

[2] Y. Wang, R. Fu, Y. Ye, U. Khan and K. Pahlavan "Performance Bounds for RF Positioning of Endoscopy Camera Capsules" in the *IEEE Radio Wireless Week 2011*

[3] F. Askarzadeh, Y. Ye, U. Khan, F. Akgul, K. Pahlavan and S. Makarov "Computational Methods for Localization," Chapter for *Position Location – Theory, Practice and Advances: A handbook for Engineers and Academics By S. Zekavat and M. Beuhrer*.

[4] K. Sayrafian-Pour, W.-B. Yang, J. Hagedorn, J. Terrill, and K. Yazdandoost, "A statistical path loss model for medical implant communication channels," in *Personal, Indoor and Mobile Radio Communications,2009 IEEE 20th International Symposium on*, 13-16 2009, pp. 2995 –2999.

[5] Makoto Kawasaki, Ryuji Kohno "A TOA based Positioning Technique of Medical Implanted Devices," *Third International Symposium on Medical Information & Communication Technology.* February 2009

[6] K. Pahlavan, F. Akgul, Y. Ye, T. Morgan, F. A.-Shabdiz, M. Heidari, C. Steger, "Taking Positioning Indoors: Wi-Fi Localization and GNSS", *Inside GNSS, vol. 5, no. 3, May, 2010.*